Chemical Physics Letters 535 (2012) 111–115

Contents lists available at SciVerse ScienceDirect

Chemical Physics Letters

journal homepage: www.elsevier.com/locate/cplett

Transport spin polarization of magnetic C_{28} molecular junctions

Ke Xu [a], Jing Huang [a,b], Zhaoyong Guan [a], Qunxiang Li [a,*], Jinlong Yang [a]

[a] Hefei National Laboratory for Physical Sciences at Microscale, University of Science and Technology of China, Hefei, Anhui 230026, People's Republic of China
[b] School of Materials and Chemical Engineering, Anhui University of Architecture, Hefei, Anhui 230022, People's Republic of China

ARTICLE INFO

Article history:
Received 2 February 2012
In final form 19 March 2012
Available online 28 March 2012

ABSTRACT

We present a theoretical study of spin transport through a magnetic C_{28} molecule sandwiched between two Au (1 1 1) electrodes. The *ab initio* modeling is performed by spin density functional theory and non-equilibrium Green's function technique. The results clearly show that the spin-resolved transmission spectra of C_{28} molecular junctions exhibit robust transport spin polarization (TSP) characteristics, which depends on the contact configuration. At the small bias voltage, the conductance of C_{28} is mainly determined by the spin-down electrons. The TSP behavior can be effectively tuned by the gate. Our results indicate that C_{28} molecule holds promise in future molecular spintronics applications.

1. Introduction

In the past years, significant progress in designing, controlling, and understanding the electronic transport properties in molecular-scale systems has been achieved, leading to the demonstration of molecular electronics, such as molecular transistors, diodes, and wires [1–5]. Recently, molecular spintronics, in which molecules are used as spin transport channel, has attracted enormous research attentions since it holds promise for the next generation of electronic devices with enhanced functionality and improved performance, especially in high-density information storage and quantum computing [6–8]. Among various potential molecular candidates, fullerenes form a promising family of compounds owing to its unique cage structure and fanciful electronic structures. The transport properties of many fullerenes including C_{60} [9–11], $C_{59}N$ [12–14], $C_{59}B$ [13,14], and C_{20} [15] have been extensively investigated. However, the knowledge of the spin-resolved transport properties through the small fullerenes molecules (<C_{60}) is still limited so far.

As one of the smallest fullerenes, C_{28} molecule, as illustrated in Figure 1a, will favor a tetrahedral cage with four unpaired electrons in an $^5A_2$ open-shell ground state of T_d symmetry [16,17]. Since C_{28} molecule is very active, it can form particularly stable endohedral complexes with tetravalent metal atoms such as C, Si, Ge, Sn, Ti, Zr, Hf, and U [19–21]. Another way to stabilize C_{28} is to saturate the four singly occupied orbitals (p-like) with four exohedral atoms (i.e. H and Cl) [18]. Previous experimental and theoretical investigations mainly focused on its stability, electronic structure, and superconductivity of C_{28} and its derivatives [22–25]. To our knowledge, the transport behavior of C_{28} is not reported so far. In this Letter, we examine the spin-resolved transport properties of C_{28} molecule sandwiched between Au (1 1 1) electrodes with different contact configurations. Our calculations clearly demonstrate the robust transport spin polarization (TSP) in three C_{28} molecular junctions, and the TSP can be effectively tuned by the gate voltage.

2. Computational methods

In our calculations, geometry relaxations and electronic structures are calculated by using SIESTA package [26] with generalized gradient approximation in the Perdew–Burke–Ernzerhof form [27]. A double-ζ plus polarization basis set is employed to describe the localized atomic orbitals. The core electrons are modeled with Troullier–Martins nonlocal pseudopotential [28]. An energy cutoff for real-space mesh size is set to be 400 Ry. All atomic positions are fully relaxed with a force tolerance of 0.01 eV/Å.

The spin-resolved transport properties of C_{28} molecular junctions are studied by the real-space nonequilibrium Green's function (NEGF) technique in combination with spin-dependent density functional theory (DFT) calculations implemented in the ATK package [29,30]. This NEGF + DFT methodology has been adopted to explain various experimental results successfully [31–33]. The spin-polarized current–voltage (I–V) curves are obtained by using the Landauer–Büttiker formula as

$$I(V) = \frac{e}{h}\int T_\sigma(E,V)[f(E-\mu_L) - f(E-\mu_R)]dE, \quad (1)$$

here, $T_\sigma(E,V)$ is transmission functions for the spin-up and spin-down electrons ($\sigma = \uparrow / \downarrow$), defined as $T_\sigma(E,V) = Tr[\Gamma_L G_\sigma \Gamma_R G_\sigma^+]$, G_σ is the spin-dependent retarded Green's function of the extended molecule, $\Gamma_{L/R}$ is the coupling matrix between the scattering region

* Corresponding author. Fax: +86 551 3602969.
E-mail address: liqun@ustc.edu.cn (Q. Li).

0009-2614/$ - see front matter © 2012 Elsevier B.V. All rights reserved.
http://dx.doi.org/10.1016/j.cplett.2012.03.066

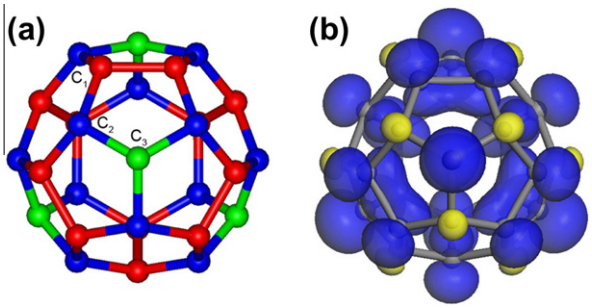

Figure 1. (a) The optimized structure of C_{28} molecule. The red, blue and green balls stand for three types of inequivalent C atoms, named as C_1, C_2 and C_3, respectively. (b) Spin density distribution of free C_{28} molecule. Here, the values of the blue and cyan isosurfaces are all set to be 0.04 and −0.04 e/Å^3, respectively. (For interpretation of the references to colour in this figure legend, the reader is referred to the web version of this Letter.)

Table 1
The symmetries, and energies (in eV), and population analysis (C_1:C_2:C_3, in%) spin-resolved frontier molecular orbitals of C_{28}.

	HOMO − 2	HOMO − 1	HOMO	LUMO
Symmetry	T_1	T_2	A_1	E
Energy	−5.39	−5.12	−5.07	−2.26
Population	33:63:4	63:19:18	27:15:58	33:62:5
	HOMO − 1	HOMO	LUMO	LUMO + 1
Symmetry	A_1	T_1	T_2	A_1
Energy	−7.46	−5.29	−4.24	−3.80
Population	27:56:17	29:67:4	63:19:18	27:15:58

and the left/right electrode, $f(E-\mu_{L(R)})$ is the Fermi function, and $\mu_{L/R}$ stands for the chemical potential of left/right electrode, respectively.

To save computational time of the spin transport calculations, a mesh cutoff is set to be 150 Ry and the Monkhorst–Pack [34] (1 × 1) K-point grid is used to sample the 2D Brillouin zone. Test calculations with the larger basis set size, larger cutoff energy, and dense K-point (i.e. 3 × 3) are also performed, which give similar results.

3. Results and discussions

As shown in Figure 1a, the optimized ground structure of C_{28} molecule with T_d symmetry has four hexagons and twelve pentagons. There are three types of inequivalent C atoms labeling with C_1, C_2 and C_3 in Figure 1a. The number of C_1, C_2 and C_3 atoms is 12, 12 and 4, respectively. The nearest neighboring interatomic C_1–C_2, C_2–C_3, and C_1–C_3 distances is 1.41, 1.44 and 1.49 Å, respectively, which are close to the previous reported values [17]. The spin-density of C_{28} is plotted in Figure 1b. It is clear that the spin-density distribution on three types of inequivalent C atoms is obvious different, and the mainly localizes at C_3 atoms. The calculated local atomic magnetic moment of C_1, C_2 and C_3 atoms is 0.26, −0.07, and 0.45 μ_B, respectively. The molecular magnetic moment of C_{28} is predicted to be 4.0μ_B, which agrees well with previous reports [17,18]. Table 1 summaries the symmetries, energy levels and population analysis of the selected frontier molecular orbitals of C_{28}. Clearly, the energies of these molecular orbitals of the spin-up and spin-down electrons are remarkably different. For the spin-up electrons, the highest occupied molecular orbital (HOMO) with A_1 symmetry and the lowest unoccupied molecular orbital (LUMO) with E symmetry locates at −5.07 and −2.26 eV, while for the spin-down electrons, the HOMO with T_1 symmetry and LUMO with T_2 symmetry lies at −5.29 and −4.24 eV, respectively. It turns out that the energy gap between the HOMO and LUMO of the spin-up and spin-down electrons is 2.81 and 1.05 eV, respectively. Moreover, the relative contribution from three types of inequivalent C atoms to the frontier molecular orbitals is significantly different. The HOMO and LUMO of the spin-up electrons is mainly contributed by C_3 and C_2 atoms, while the HOMO and LUMO of the spin-down electrons is dominated by the C_2 and C_1 atoms, respectively. Note that C_3 atom has relative small contribution to the HOMO of the spin-down electrons and the LUMO of the spin-up electrons. These observations imply that C_{28} molecule with large magnetic moment (4.0 μ_B) is potential candidate for molecular spintronics.

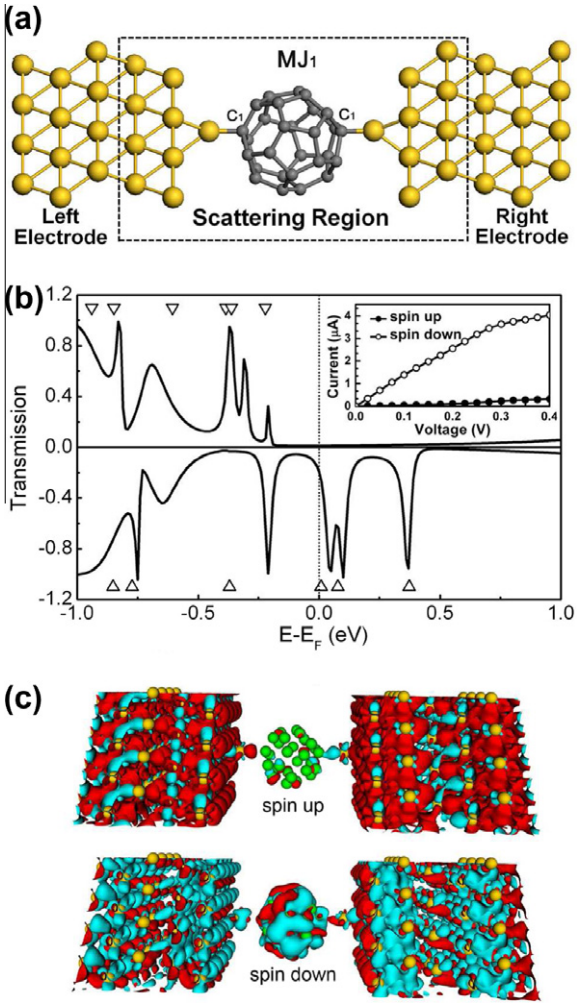

Figure 2. (a) Computational model for the proposed molecular spin filter (MJ_1). Here, C_{28} molecule is coupled to two Au (1 1 1) surfaces through C_1-Au end connections, and the atom species are identified by color. (b) The spin-resolved transmission spectra of the MJ_1 junction, and the inset shows the I–V curves. (c) The profile of the spin-resolved local density of states of MJ_1 at the Fermi level. (For interpretation of the references to colour in this figure legend, the reader is referred to the web version of this Letter.)

In molecular electronics, contact configurations are typical factors to affect their transport properties [9,15,35,36]. We therefore examine three C_{28} molecular junctions, namely with MJ_1, MJ_2, and MJ_3, where the C_{28} molecule couples to the Au (1 1 1) electrodes with C_1–Au, C_2–Au or C_3–Au end connections, respectively. Two Au adatoms in the right and left electrodes are adopted in three examined junctions to reduce the strong molecule–electrode interaction due to the small C_{28} molecular radius. The optimized anchoring C–Au distances in three molecular junctions is very close (about 2.25 Å), and the distance between Au adatom and the nearest neighboring

Au atom of Au (1 1 1) surface is about 2.24 Å. Figure 2a illustrates the proposed C_{28} junction (MJ_1). The examined molecular junction can be divided into three parts: the scattering region, left and right electrodes. The scattering region is modeled with a $11.54 \times 11.54 \times 20.59$ Å unit cell. Figure 2b shows the spin-resolved zero-bias transmission spectra of MJ_1 within the energy window from −1.0 to 1.0 eV. Here, the Fermi level is set as zero for clarity, and the empty triangles stand for the molecular projected self-consistent Hamiltonian (MPSH) eigenvalues. The MPSH eigenstates can be referred as perturbed C_{28} molecular orbitals (MOs) because of the presence of Au electrodes [29]. As we can see, C_{28} retains its spin polarization in the junction. The energy positions of the perturbed MOs relative to the Fermi level match well with the transmission peaks. The remarkably difference of the conductance behavior of two spin channels is observed. As for the spin-up (majority) electrons, there are several transmission peaks below the Fermi level, and above the Fermi level the transmission coefficients are very small and the transmission spectrum shows flat feature. Upon the spin-down electrons, several significant transmission peaks locates at −0.21, 0.05, and 0.10 eV.

In order to quantitatively measure the spin filtering efficiency (SFE), we define the transport spin polarization at the Fermi level as $\mathrm{SFE} = [T_\uparrow(E_F) - T_\downarrow(E_F)]/[T_\uparrow(E_F) + T_\downarrow(E_F)]$, where $T_\uparrow(E_F)$ and $T_\downarrow(E_F)$ stand for the transmission coefficient of the spin-up and spin-down electrons at the Fermi level. A positive (negative) value of the SFE denotes a conductance dominated by the spin-up (spin-down) channel. The calculated transmission coefficients of two spin channels ($T_\uparrow$ and $T_\downarrow$) through the Mol_1 at the Fermi level is about 1.15×10^{-2} and 0.19, respectively, and the SFE of MJ_1 at the Fermi level is predicted to be −88.7%. This conductance dominated by the spin-down electrons has been observed in the iron-cyclooctatetraene (Fe–COT) clusters [37], vanadium–benzene (V–Bz) clusters [38], manganese phthalocyanine (MnPc) and FePc molecules [39–41]. As shown in Figure 2c, at the Fermi level electronic states of the spin-down electrons are almost distributed over the whole system thus a large transmission conductance is obtained, while for the spin-up electrons there are hardly any electronic states on the anchoring C–Au bonds. These results indicate that C_{28} molecule sandwiched between Au electrodes acts as a nearly perfect spin filter.

Actually, this spin-filtering device can works at finite bias voltage. The spin-resolved *I–V* curves through C_{28} are calculated and plotted in inset of Figure 2b. The currents of the spin-down electrons through C_{28} molecule increase monotonously with the applied bias voltage, and its values are significant larger than that of the spin-up electrons. The calculated spin-up (spin-down) current at 0.4 V through C_{28} is 0.32 (4.04) μA. The current difference between the spin-up and spin-down electrons under different bias voltage can be quantified by the ratio of current defined as $R(V) = |I_\downarrow(V)/I_\uparrow(V)|$. The calculated *R* varies from 13 to 31 in the examined bias range. Such a large ratio in this given range of bias voltage can be readily measured and is desirable for the real application.

Now we turn to explore the effect of contact configurations on the transport properties through C_{28} molecule. Figure 3a and b show the spin-resolved transmission spectra of MJ_2 and MJ_3, respectively. It is clear that the transport behavior of MJ_2, in which two Au adatoms connect to the C_2 atoms, is similar to that of MJ_1. At the Fermi level, the transmission coefficients for the spin-down electrons are significantly larger than that of the spin-up electrons. The SFE of MJ_2 is predicted to be about −96.7%, which indicates that transport properties of MJ_2 is also primarily determined by the spin-down electrons. When C_{28} molecule couples to Au (1 1 1) surfaces via the C_3–Au connections in MJ_3, obvious transport spin polarization is observed, as shown in Figure 3b. For the spin-down electrons, a significant transmission peak labeled with ∗ locates at

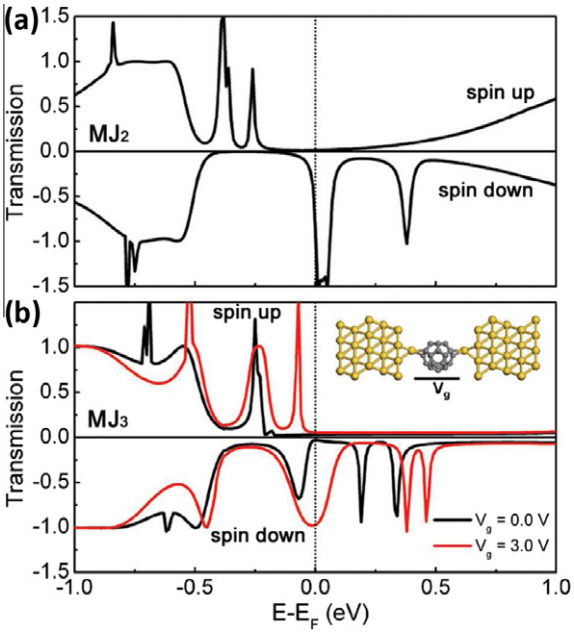

Figure 3. The spin-resolved transmission spectra of the C_{28} junctions with different contact configuration. (a) MJ_2, (b) MJ_3. Here, the red solid lines stand for the transmission curves of the MJ_3 junction under 3.0 V gate voltage. (For interpretation of the references to colour in this figure legend, the reader is referred to the web version of this Letter.)

−0.07 eV, while the transmission coefficients in the energy range from −0.21 to 1.0 eV are negligible. However, the SFE at the Fermi level is only about −5.0%, which blocks its application in molecular spintronics. To increase the SFE of MJ_3 junction, we consider the gate effect since previous theoretical investigations have shown that the transport behavior of a single-molecule can be effectively modulated by applying a gate electrode [42,43]. In our calculations, the applied gate voltage simply shifts the MPSH energy levels through inducing an electrostatic potential localized to the molecular region and it does not change the C_{28}-electrode couplings. The spin-resolved transmission spectra of MJ_3 under gate voltage ($V_g = 3.0$ V) as an example is plotted in Figure 3b with solid red lines. Clearly, the shape of transmission spectra and position of peaks are obviously tuned by the gate voltage. The transmission peak (labeled with ∗ without applying gate voltage) of the spin-down electrons become broaden and crosses the Fermi level, while the transmission coefficient of the spin-up electrons at the Fermi level is still very small. It leads to a high SFE (about −90.0%) in MJ_3 by the 3.0 V gate voltage.

To understand the different transport properties of three C_{28} molecular junctions, we perform the Mulliken population and magnetic moment (MM) analysis, and calculate the density of states (PDOS) of these examined junctions. The DOS of the C_{28} and the partial DOS of the Au adatoms are plotted in Figure 4. It is clear that the spin-polarized transmission spectrum generally follows the calculated PDOS of the spin-up and spin-down electrons, especially of transmission peak. This indicates that the spin transport properties of three molecular junctions are mainly determined by the sandwiched C_{28} molecule. These large peaks of transmission curve originate from resonant transmission through the molecular states. Due to the molecule-electrode interaction, the charge transfer is about 0.25 e transferring from the electrodes to the C_{28}, which is not sensitive to the contact configuration. The C_{28} molecular MM in the junctions is highly reduced compared to those of the free molecule (4.0 μ_B). The MM is about 2.63, 2.88, and 2.41 μ_B in MJ_1, MJ_2, and MJ_3, respectively. The similar

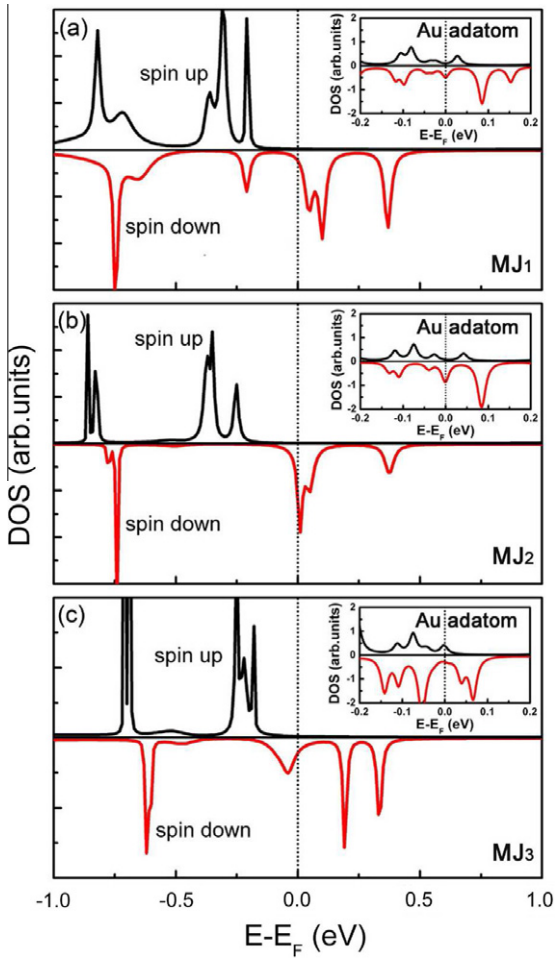

Figure 4. Spin-polarized DOS of the sandwiched C_{28} molecule in the MJ_1 (a), MJ_2 (b), and MJ_3 (c) junctions. The insets stand for the corresponding partial DOS of the Au adatoms in three examined molecular junctions.

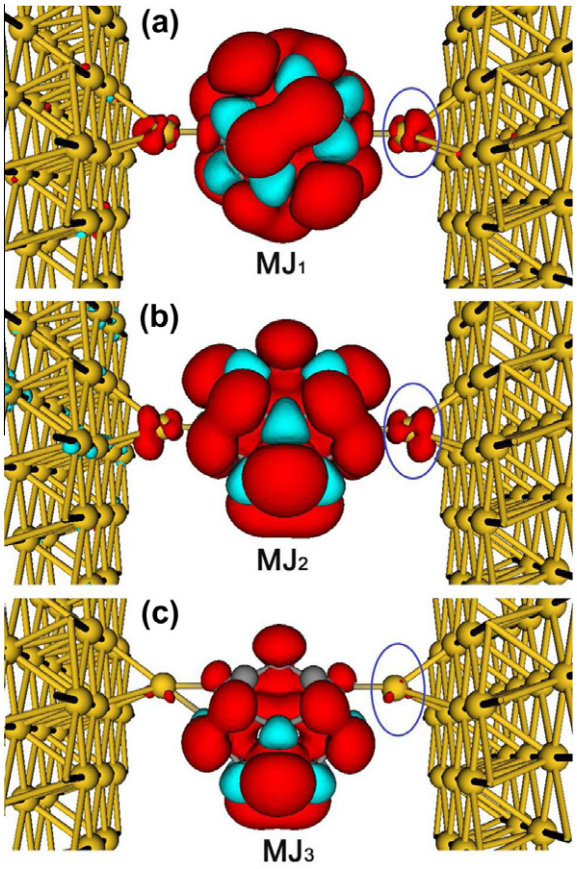

Figure 5. Spin density distribution of three examined C_{28} molecular junctions: (a) MJ_1, (b) MJ_2, and (c) MJ_3. The values of the red and cyan isosurfaces are set to be 0.003 and −0.003 e/Å^3, respectively. (For interpretation of the references to colour in this figure legend, the reader is referred to the web version of this Letter.)

reduction of the molecular MM have been observed in the N@C_{60} molecule by the carrier doping [44] and edge chemical modification [45]. Note that the atomic MMs of the end connecting C atoms (C_1, C_2 and C_3) of the C_{28} are almost quenched (the MMs are all less than $0.1\mu_B$), while the Au adatoms are obviously spin-polarized, as shown in the insets of Figure 4.

As mentioned above, the contact configurations have a noticeable effect on the electron transport characteristics of the examined molecular junctions [9,15,35,36,46]. We find that the partial DOS of the Au adatoms are remarkably different for three different contact configurations. They are consistent well with the spin-polarized transmission spectra of MJ_1 (Figure 2b), MJ_2 and MJ_3 (Figure 3). Figure 5 plots the calculated spin density distribution of three examined C_{28} molecular junctions. The unpaired electrons are largely localized on the C_{28} cage, however, the spin density distribution at the Au adatoms are remarkably different. In the MJ_1 and MJ_2 junctions notable spin density distributes at the Au adatoms, while the spin density on the Au adatom in MJ_3 is negligible. Clearly, in the term of the calculated DOS and spin density results, it is easy to understand the different spin transport properties of the C_{28} junctions with three different contact configurations.

The presented theoretical results imply that C_{28} molecule can be used as a promising candidate for future molecular spintronic devices. However, it should be pointed out that an isolated C_{28} molecule with T_d symmetry is composed of well-separated dangling bonds (spin 1/2 centers) and the C atom has weak spin–orbit coupling effects. An external magnetic field is required to form a stable spin-ordering mainly through the Heisenberg exchange coupling in C_{28} molecule [47]. That is to say, one has to bias the C_{28} molecular junction with an applied magnetic field to probe the interesting spin-dependent transport in experiments.

4. Summary

In summary, we explore the spin transport properties of the C_{28} molecular junctions by using DFT calculations and NEGF techniques. Three different contact configurations are examined. The spin-resolved transmission spectra of three examined C_{28} molecular junctions depend on the contact configuration and exhibit robust TSP. At the small bias voltage, the transport property of C_{28} is mainly determined by the spin-down electrons. Moreover, such TSP behavior can be effectively tuned by the gate voltage. The presented theoretical results imply that C_{28} molecule can be used as a promising candidate for future molecular spintronics devices.

Acknowledgments

This work is partially supported by the National Basic Research Program of China (No. 2011CB921404), by the National Natural Science Foundation of China (Nos. 11074235, 11034006, 20903003), by the Knowledge Innovation Program of the Chinese Academy (No. KJCX2-YW-W22), by the Fundamental Research Funds for the Central Universities (No. WK2340000007), and

Supercomputing Center of USTC, and by Shanghai Supercomputer Center.

References

[1] N.J. Tao, Nat. Nanotechnol. 1 (2006) 173.
[2] R.L. McCreery, A.J. Bergren, Adv. Mater. 21 (2009) 4303.
[3] W.Y. Kim, K.S. Kim, Acc. Chem. Res. 43 (2010) 111.
[4] H. Song, M.A. Reed, T. Lee, Adv. Mater. 23 (2011) 1583.
[5] N.A. Zimbovskayaa, M.R. Pederson, Phys. Rep. 509 (2011) 1.
[6] S.A. Wolf et al., Science 294 (2001) 1488.
[7] A.R. Rocha, V.M. García-suárez, S.W. Bailey, C.J. Lambert, J. Ferrer, S. Sanvito, Nat. Mater. 4 (2005) 335.
[8] S. Sanvito, Chem. Soc. Rev. 40 (2011) 3336.
[9] H.Y. He, R. Pandey, S.P. Karna, Chem. Phys. Lett. 439 (2007) 110.
[10] N. Sergueev, A.A. Demkov, H. Guo, Phys. Rev. B 75 (2007) 233418.
[11] X.H. Zheng, W.C. Lu, T.A. Abtew, V. Meunier, J. Bernholc, ACS Nano 4 (2010) 7205.
[12] J. Zhao et al., Phys. Rev. Lett. 95 (2005) 045502.
[13] X.L. Zhong, R. Pandey, A.R. Rocha, S.P. Karna, J. Phys. Chem. Lett. 1 (2010) 1584.
[14] X.J. Zhang, M.Q. Long, K.Q. Chen, Z. Shuai, Q. Wan, B.S. Zou, Y. Zhang, Appl. Phys. Lett. 94 (2009) 073503.
[15] L.H. Wang, Y. Guo, C.F. Tian, X.P. Song, B.J. Ding, J. Appl. Phys. 107 (2010) 103702.
[16] T. Guo et al., Science 257 (1992) 1661.
[17] T. Guo, R.E. Smalley, G.E. Scuseria, J. Chem. Phys. 99 (1992) 352.
[18] H.W. Kroto, D.R.M. Walton, Chem. Phys. Lett. 214 (1993) 353.
[19] M.R. Pederson, N. Laouini, Phys. Rev. B 48 (1993) 2733.
[20] K. Jackson, E. Kaxiras, M.R. Pederson, Phys. Rev. B 48 (1993) 17556.
[21] J.P. Dognon, C. Clavaguéra, P. Pyykkö, J. Am. Chem. Soc. 131 (2009) 238.
[22] P.R.C. Kent, M.D. Towler, R.J. Needs, G. Rajagopal, Phys. Rev. B. 62 (2000) 15394.
[23] A. Enyashin, S. Gemming, T. Heine, G. Seifert, L. Zhechkov, Phys. Chem. Chem. Phys. 8 (2006) 3320.
[24] N.A. Romero, J. Kim, R.M. Martin, Phys. Rev. B 76 (2007) 205405.
[25] X. Lu, Z.F. Chen, Chem. Rev. 105 (2005) 3643.
[26] J.M. Soler, E. Artacho, J.D. Gale, A. García, J. Phys. Condens. Matter 14 (2002) 2745.
[27] J.P. Perdew, K. Burke, M. Ernzerhof, Phys. Rev. Lett. 77 (1996) 3865.
[28] N. Troullier, J.L. Martins, Phys. Rev. B. 43 (1991) 1993.
[29] J. Taylor, H. Guo, J. Wang, Phys. Rev. B 63 (2001) 245407.
[30] M. Brandbyge, J.L. Mozos, J. Taylor, K. Stokbro, Phys. Rev. B 65 (2002) 165401.
[31] S.K. Nielsen, M. Brandbyge, K. Hansen, K. Stokbro, J.M. van Ruitenbeek, F. Besenbacher, Phys. Rev. Lett. 89 (2002) 066804.
[32] X.J. Wu, Q.X. Li, J. Huang, J.L. Yang, J. Chem. Phys. 123 (2005) 184712.
[33] J. Huang, Q.X. Li, Z.Y. Li, J.L. Yang, J. Nanosci. Nanotechnol. 9 (2009) 774.
[34] H.J. Monkhorst, J.D. Pack, Phys. Rev. B. 13 (1976) 5199.
[35] Z.Y. Li, D.S. Kosov, J. Phys. Chem. B 110 (2006) 19116.
[36] H. Hao, X.H. Zheng, Z.X. Dai, Z. Zeng, Appl. Phys. Lett. 96 (2010) 192112.
[37] J. Huang, Q.X. Li, K. Xu, H.B. Su, J.L. Yang, J. Phys. Chem. C 114 (2010) 11946.
[38] M. Koleini, M. Paulsson, M. Brandbyge, Phys. Rev. Lett. 98 (2007) 197202.
[39] X. Shen, L. Sun, E. Benassi, Z. Shen, X. Zhao, S. Sanvito, S.M. Hou, J. Chem. Phys. 132 (2010) 054703.
[40] X. Shen et al., Phys. Chem. Chem. Phys. 12 (2010) 10805.
[41] J. Huang, K. Xu, S.L. Lei, H.B. Su, S.F. Yang, Q.X. Li, J.L. Yang, J. Chem. Phys. 135 (2012) 064707.
[42] A.A. Farajian, R.V. Belosludov, H. Mizuseki, Y. Kawazoe, T. Hashizume, B.I. Yakobson, J. Chem. Phys. 127 (2007) 024901.
[43] J. Huang, Q.X. Li, H.B. Su, J.L. Yang, Chem. Phys. Lett. 479 (2009) 120.
[44] J.E. Grose et al., Nat. Mater. 7 (2008) 884.
[45] G.Q. Liu, A.N. Khlobystov, A. Ardavan, G.A.D. Briggs, K. Porfyrakis, Chem. Phys. Lett. 508 (2011) 187.
[46] Z.L. Li, B. Zou, C.K. Wang, Y. Luo, Phys. Rev. B 73 (2006) 075326.
[47] A.V. Postnikov, Jens Kortus, M.R. Pederson, Phys. Stat. Sol. (b) 243 (2006) 2533.